Convective nature of planimetric instability in meandering river dynamics.

Convective nature of the planimetric instability in meandering river dynamics

Carlo Camporeale* and Luca Ridolfi†
Department of Hydraulics, Politecnico di Torino, Italy
(Received 4 August 2005; published 28 February 2006)

The convective nature of the linear instability of meandering river dynamics is analytically demonstrated and the corresponding Green's function is derived. The wave packet due to impulsive disturbance migrates along a river either downstream or upstream, depending on the subresonant or superresonant conditions. The influence of the parameters that govern the meandering process is shown and the role of the fluid dynamic detail used to describe the morphodynamic problem is discussed. A numerical simulation of the river planimetry is also developed.

DOI: 10.1103/PhysRevE.73.026311 PACS number(s): 47.20.−k, 47.54.−r, 92.40.Qk

I. INTRODUCTION

Meandering rivers are far-from-equilibrium systems which are driven by morphodynamic instabilities. Over the last few decades, several works have improved knowledge on the complex morphodynamic interactions that occur between a turbulent stream and an erodible bed (e.g., see the reviews by Ikeda and Parker [1] and Seminara [2]). It has been recognized that the core mechanism of meandering is the action of a helicoidal curvature-driven secondary flow which activates an inward lateral sediment flux [3,4]. The consequent transversal shoaling of the bed, with the formation of point bars, triggers a topography-driven secondary flow and a topographic steering of the longitudinal flow [5], which in turn induces outward bank erosion. The longitudinal transport of momentum induces a streamwise phase lag between the curvature and the flow field, that establishes a spatial memory in the downstream propagating influence [6] and, consequently, in both the downstream skewness in the shape of the meander loops and in the downstream planimetric migration [7]. Curvature therefore increases and the process is self-sustained. Finally, for particular geometric conditions, the interaction between the planimetric response and the bed response leads to resonant behavior [8].

From the previously mentioned picture, it emerges that a shallow water flow on an erodible bed is unstable and can develop a meandering planimetry. This has been shown in literature through normal mode analysis applied to some linear meandering dynamics models, whose level of fluid dynamic detail can generally be summarized by the order of the linear differential equation that describes the flow field. Ikeda *et al.* [9] and Edwards and Smith [10] investigated the wave-number range of instability in the context of a first-order linear model; similarly, the speculations by Parker and Johannesson [11], regarding the resonance condition for a second-order linear model, can be related to the detection of the maximum instability response. Finally, Seminara *et al.* [12] imposed a normal mode decomposition to solve the planimetric evolution numerically with the use of a fourth-order linear model.

Although the previous works have led to many important advances, it has still to be investigated whether the planimetric instability of the meandering dynamics is of a convective or absolute type. This analysis is the subject of the present work, where the asymptotic behavior of the Green's function is also obtained and discussed. Physically speaking, an impulsive perturbation of a dynamical system produces a convective instability if the response increases, but migrates and decays to zero at all the spatial locations; on the contrary, the instability is absolute if it is unbounded throughout for a long time [13–15].

The determination of the nature of meandering instability is of both speculative and applicative interest. The former interest is stimulated by a recent work by Zolezzi and Seminara [16], where an upstream propagating influence in the flow field response, which is responsible for the upstream migration of meanders in superresonant conditions, was pointed out. This morphodynamic mechanism, along with the well-known downstream propagating influence, could make the propagation of an impulsive perturbation possible both upstream and downstream at the same time and, in this case, the instability could be absolute; otherwise, one direction could prevail and the instability would be convective. Also, it should be noted that the presence of the longitudinal downstream migration of meanders does not imply the convective nature of the instability, but only shows that the most unstable wave number has a positive velocity. Formally, the convective instability requires that all the unstable harmonics propagate in the same direction. The applicative interest instead lies in the capacity to predict whether planimetric perturbations in a straight stream—e.g., bank failures or obstructions—only affect the downstream sections, leaving the upstream portion of the river unperturbed or, on the contrary, they perform an upstream spreading which changes the whole initial configuration in the long term. Finally, the analysis of Green's function is a powerful tool to investigate the linear behavior of a dynamical system, as it is the basic element for the solution of any linear initial-boundary problem [15,17].

A similar investigation has recently been carried out, in the context of free bar instability, in the work by Federici and Seminara [18], where the authors pointed out the convective nature of the bar instability. Although closely related, bedform and planform instabilities are conceptually different.

*Electronic address: carlo.camporeale@polito.it
†Electronic address: luca.ridolfi@polito.it

The planimetric instability of a meandering river, besides the morphodynamic equations, also involves the evolution equation of the river axis. It follows that the dispersion relation is therefore mathematically very different from the bar one.

In the following, three well-known linear morphodynamic models are referred to, namely the models by Ikeda, Parker, and Sawai [9], Johannesson and Parker [19], and Zolezzi and Seminara [16] (hereafter referred as to the IPS, JP, and ZS models, respectively). These three models represent different, typical levels of simplification—giving rise to first-, second-, and fourth-order models, respectively—and have been key steps in the comprehension and modeling of meandering dynamics. Moreover, the IPS and JP models have been widely used in the numerical simulations of river evolution [20–23], while the ZS model can be considered the most detailed model in the linear approach and it encompasses all the principal morphodynamic mechanisms (for this reason, ZS is used here as reference model and its notation is extended to other models). Comparisons between the results provided by these different approaches are useful to discuss the effects of the different fluid dynamic hypothesis adopted in the models.

II. GENERAL FRAMEWORK

The dynamics of a meandering river is described by (i) an evolution equation that governs the temporal dynamics of the river axis and (ii) a morphodynamic model for the flow field and the sediment response. The evolution equation can be obtained using the formalism of the differential geometry of plane curves [24,25], under the hypothesis that the width of the river remains constant during its migration. The starting point is the equation of motion of a parametrized curve $\mathbf{r}(\alpha,t)$ that moves along the normal versor $\mathbf{n}$, i.e., $\mathbf{r}_{,t}=\mathbf{n}\zeta$, where t is the time, ζ is the local normal velocity, and α is a descriptive parameter which does not depend on time so that $\partial_{,t\alpha}=\partial_{,\alpha t}$, where the comma refers to the partial derivative (hereafter all the quantities are normalized by the river half-width b and the bulk velocity U [e.g., Ref. [11]]). Introducing the arc-length coordinate $s(\alpha,t)=\int_0^\alpha\sqrt{g}d\alpha'$—where $g(\alpha,t)$ is the metric coefficient $|(\mathbf{r}_{,\alpha})^2|$—and defining the curvature $C=|\mathbf{r}_{,ss}|$, using Serret-Frenet equations, it follows that $\partial_{,ts}-\partial_{,st}=-C\zeta\partial_{,s}$ which, with some algebra, leads to

$$\mathbf{r}_{,t}=\mathbf{n}\zeta-\mathbf{r}_{,s}\int^s C\zeta ds'. \tag{1}$$

Once the normal-to-curve velocity, $\zeta(s,t)$, is obtained, the previous integro-differential equation describes the dynamics of the curve. It should be noted that Eq. (1) is nonlinear, regardless of the mathematical form of ζ.

The functional $\zeta(s,t)$ is given by a morphodynamic model, i.e., the second ingredient of the problem. Since a linear stability analysis is being developed, linear models are referred to. These models are based on the following four hypothesis, in order to obtain significant but mathematically tractable models. (i) The fluid is assumed to be incompressible and the flow to be fully turbulent, while the sediment of the river bed is considered cohesionless and with a uniformly distributed grain diameter, d_m. (ii) Since the typical vertical scale (i.e., the water depth D) is much smaller than the characteristic horizontal scale (i.e., the river half-width b), the vertical velocity component is neglected and a hydrostatic vertical pressure distribution can be adopted. (iii) It is assumed that both the flow and bed topography instantaneously adjust to the planimetry, that is, the process is considered as quasistationary [26]. (iv) A linear dependence of the rate of the bank erosion $\zeta(s,t)$ on the excess near-bank velocity u_b is assumed; this assumption has been justified with field observations [27] and has been adopted in several models [9,19,28–30]. Point (i) supports Exner's equation for bed sediment, hypothesis (ii) justifies the use of the shallow-water equations which, thanks to point (iii), are made to be time independent. Finally, hypothesis (iv) reads $\zeta(s)=Eu_b=Eu(s,n=1)$, where n is the transversal coordinate, $u(s,n)$ is the longitudinal flow velocity ($n=1$ corresponds to the river bank), and E is a dimensionless coefficient of erodibility.

Under the previous assumptions and introducing the velocity decomposition of the flow field [3], along with the no-slip condition at the bottom and the no-stress condition at the free surface, one obtains the depth-averaged two-dimensional equations for shallow water in curvilinear coordinates and in nondimensioned form [16,19],

$$\mathcal{N}UU_{,s}+VU_{,n}+\mathcal{N}CU(V+2\varphi)+\frac{\mathcal{N}}{F^2}H_{,s}-\beta C_f+\beta\frac{\tau_s}{D}+\frac{1}{D}(UD\varphi)_{,n}=0, \tag{2}$$

$$\mathcal{N}UV_{,s}+VV_{,n}+\frac{H_{,n}}{F^2}+\beta\frac{\tau_n}{D}+\frac{\mathcal{N}}{D}(DU\varphi)_{,s}+\frac{2}{D}(VD\varphi)_{,n}+\frac{1}{D}(\varphi_1 D)_{,n}+\mathcal{N}C\varphi_2=0, \tag{3}$$

which have to be coupled with the continuity equation for the water and bed sediment [31], respectively,

$$\mathcal{N}(DU)_{,s}+(DV)_{,n}+\mathcal{N}CDV=0, \tag{4}$$

$$\mathcal{N}q_{s,s}+q_{n,n}+\mathcal{N}Cq_n=0. \tag{5}$$

In Eqs. (2)–(5), U and V are the longitudinal and transversal depth-averaged velocity, $\mathcal{N}(s)$ is the longitudinal metric factor, D is the depth, H is the free surface elevation, $\boldsymbol{\tau}$ is the bed stress vector, $\mathbf{q}$ is the volumetric vectorial bed load, C_f is the friction factor, and F is the Froude number. Moreover, $\varphi=\langle\mathcal{F}v_0\rangle$, $\varphi_1=\langle v_0^2\rangle$ and $\varphi_2=2V\varphi-U^2+\varphi_1$, where $\langle\cdot\rangle=\int_{\xi_0}^1\cdot d\xi$, ξ_0 is the vertical position at which the no-slip condition is set, $\mathcal{F}(\xi)$ is the vertical profile of velocity, and $v_0(s,n,\xi)$ is the recirculating secondary current driven by curvature and with vanishing depth average.

Zolezzi and Seminara [16] provided a linear solution of the problem (2)–(5)—i.e., the ZS model—in terms of the lateral Fourier decomposition of the longitudinal flow field perturbation, $u(s,n)=\Sigma_{m=0}^{\infty}u_m(s)\sin Mn$ [with $M=\frac{1}{2}(2m$

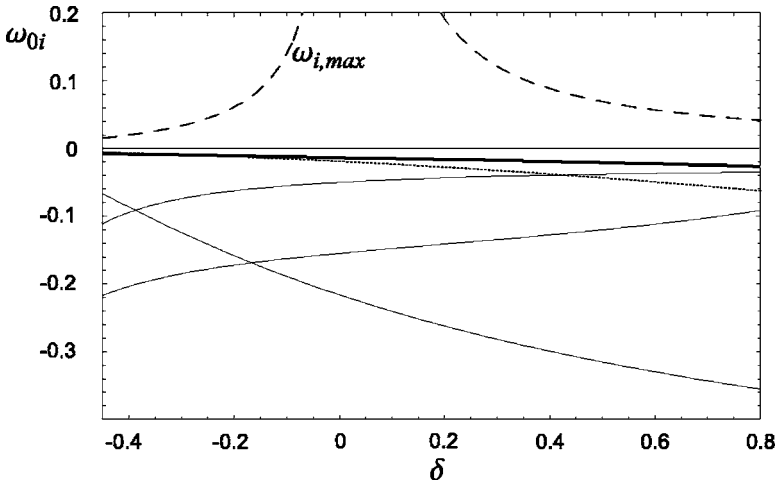

FIG. 1. Behavior of the solutions of Eq. (12) for $s/\tau=0$ vs δ, using the ZS model ($\tau^*=0.1$, $d_s=0.01$). The bold and dashed lines mark the absolute growth rate and the temporal growth rate, respectively. The JP model gives the same absolute growth rate as the ZS model (bold line), while the IPS model gives the dotted line.

$+1)\pi$]. For a longitudinally unbounded domain, the generic m mode, is described by a fourth-order ordinary differential equation (ODE) and reads

$$u_m(s) = A_m \sum_{j=1}^{N} \left[g_{j0} \int^s e^{\lambda_{mj}(s-t)} C(t)dt + \sum_{p=1}^{N} g_{jp} \frac{\partial^{(p-1)} C(s)}{\partial s^{(p-1)}} \right]. \tag{6}$$

In the previous equation $N=4$, $A_m=2(-1)^m/M^2$, and the terms g_{jk} and λ_{jm} depend on the shape ratio $\beta=b/D$, the dimensionless roughness $d_s=d_m/D$, and the Shield stress τ^*. For the convenience of the reader, the key steps of the theory by Ref. [16] are summarized in Appendix A.

Other linear models can be hierarchically derived from the same scheme and differentiate according to the neglected morphodynamic mechanisms. For example, the JP model can be obtained if three main simplifications are introduced: (i) negligible coupling between curvature-driven secondary currents and topography; (ii) no spatial variations in the friction coefficient and no dependence of the bedload transport on the flow depth; and (iii) vertically averaged value of the eddy viscosity. With these assumptions, the morphodynamic model reduces to a second-order ODE and the solution is still formally described by Eq. (6) by setting $N=2$. Similarly, if the coupling between the sediment dynamics and fluid dynamics is also neglected, and the bed topography only depends on the local curvature, the IPS model, which corresponds to Eq. (6) with $N=1$, is obtained.

III. THE NATURE OF INSTABILITY

The analysis of the convective or absolute nature of the morphodynamic instability requires the dispersion relation. For this purpose, the vectorial Eq. (1) is transformed into a scalar equation. Let us define the angle θ between the versor $\mathbf{t}$ tangential to the river axis and the horizontal, so that the following relationships apply [32]:

$$\mathbf{r}_{,ss} = \mathbf{n}\theta_{,s}, \quad \mathbf{r}_{,st} = \mathbf{n}\theta_{,t}, \tag{7a}$$

$$\mathbf{n}_{,s} = -\theta_{,s}\mathbf{r}_{,s}, \quad C = -\theta_{,s}. \tag{7b}$$

By deriving Eq. (1) with respect to s, substituting relationships (7), and scalar multiplying by $\mathbf{n}$, one obtains

$$\theta_{,t} = \zeta_{,s} + \theta_{,s} \int^s \theta_{,s'} \zeta ds'. \tag{8}$$

(the same equation was also derived by Seminara *et al.* [12] using a different approach).

It should be noticed that after linearization around the straight solution (i.e., $\theta=0$), the previous equation loses the integral term on the right-hand side. Therefore, substituting (6) in (8) and rescaling the time according to $\tau=tE$, the equation that regulates the spatiotemporal linear planimetric dynamics of the river is obtained,

$$\frac{\partial\theta}{\partial\tau} + \sum_{m=0}^{\infty} \left[A'_m \sum_{j=1}^{N} \left(g_{j0}\lambda_{mj} \int^s e^{\lambda_{mj}(s-s')} \frac{\partial\theta}{\partial s'} ds' + \sum_{p=0}^{N} g_{jp} \frac{\partial^{(p+1)}\theta}{\partial s^{(p+1)}} \right) \right] = 0, \tag{9}$$

with $A'_m=(-1)^m A_m$.

The Fourier transform with respect to s and τ of Eq. (9) readily provides the normal modes in the form of a generalized complex dispersion relation

$$\omega = k \sum_{m=0}^{\infty} \left\{ A'_m \sum_{j=1}^{N} \left[\frac{g_{j0}\lambda_{mj}}{ik - \lambda_{mj}} + \sum_{p=0}^{N} g_{jp}(ik)^p \right] \right\}, \tag{10}$$

where ω and k are the complex dimensionless frequency and wave number, respectively.

The absolute or convective instability criterion, as summarized by Huerre and Monkevitz [33], who extended the concepts introduced by Briggs [34] and Bers [13] to shear flow instabilities, can now be applied. According to Bers [13], a convective instability leads Green's function to decay asymptotically to zero along the ray $s/\tau=0$, vice versa, in absolute instabilities, the response tends to infinity. For this purpose, each spatiotemporal ray $s/\tau=V$ can be analyzed recalling the saddle-point condition

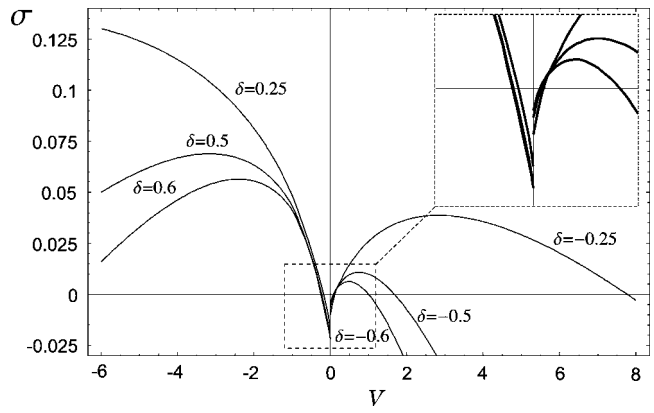

FIG. 2. Temporal growth rates vs the ray velocity $V=s/\tau$ for different values of δ ($\tau^*=0.1$, $d_s=0.01$).

$$\frac{\partial\omega(k)}{\partial k}=\frac{s}{\tau}. \tag{11}$$

The complex *absolute wave number* k_0 being the solution of Eq. (11) for the ray $s/\tau=0$, and $\omega_{0i}=\mathrm{Im}[\omega(k_0)]$ the associated *absolute growth rate*, the theory states that the temporal growth rate along each ray $s/\tau=V$ is $\sigma(V)=\omega_{0i}-Vk_{0i}$ (hereafter the subscript i refers to the imaginary part). Furthermore, if just real wave numbers are considered, equation $\partial\omega_i/\partial k=0$ provides the wave number k_{max} which displays the maximum temporal growth rate $\omega_{i,max}=\omega_i(k_{max})$ with the corresponding group velocity $V_{max}=\partial\omega/\partial k(k_{max})$. In short, the aforementioned criterion states that the instability is convective if $\omega_i(k_{max})>0$ and $\omega_{0i}<0$. On the contrary, the flow is absolutely unstable if $\omega_i(k_{max})>0$ and $\omega_{0i}>0$, provided the *casuality principle* is satisfied. The latter principle requires that the complex k-plane displays the pinching point k_0 between two branches $k^+(\omega)$ and $k^-(\omega)$ of the dispersion relation confined well within their respective half-k planes when $\omega_i \gg \omega_{0i}$ [15,33].

Let us consider the most refined linear meandering model, i.e., the ZS one ($N=4$). The nature of instability can be investigated just considering the contribution given by the leading lateral mode, that is, $m=0$ in Eq. (10). The higher modes in fact do not introduce any qualitative novelty to the outcome (see the next section). Figure 1 shows the solutions of Eq. (11) with $s/\tau=0$, varying the ratio $\delta=(\beta-\beta_R)/\beta_R$, where β_R is the aspect ratio at resonant conditions. As Eq. (11) is a tenth-order algebraic equation, just the physically significant roots have been plotted in the figure and the multiple ones have been left out. The maximum temporal growth rate $\omega_{i,max}$ is also displayed with a dashed line. From this picture, the meandering planimetry process results to be convectively unstable, since all the roots are negative. The same outcome can be obtained with different settings of the Shield stress, τ^* (with $\tau^*<0.4$), and the relative roughness, d_s. We can notice that the present result does not require any further analysis involving the pinching process, since the casuality principle is automatically satisfied in the case of the convective instabilities. However, the pinching process has been applied to detect which of the roots shown in Fig. 1 corresponds to ω_{0i}, in order to exclude the *marginally absolute* instability (i.e., $\omega_{0i}=0$) and to obtain Green's function, as will be shown in the next section.

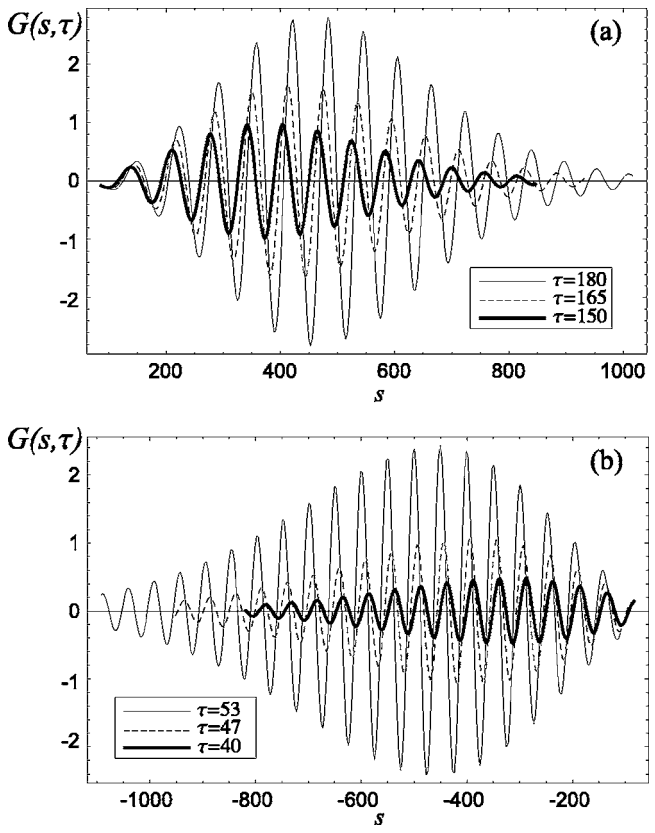

FIG. 3. Green's function evolution provided by the ZS model ($\tau^*=0.1$, $d_s=0.01$). (a) Subresonant case ($\delta=-0.25$), (b) superresonant case ($\delta=0.25$). Abscissa and ordinates appear in different scales.

The result for the fourth-order model is compared with the ω_{0i} values provided by the second and first-order models. The latter in particular leads to the analytical expression

$$\omega_{0i}=\frac{-27a^3+9a^2(\varphi-3b)-b^2(b+\varphi)+ab(4\varphi-b)}{4(a+b+\varphi)}, \tag{12}$$

where $a=-\lambda_1$, $b=g_{10}+\lambda_1$, and $\varphi=\sqrt{9a^2+10ab+b^2}$. If the IPS model is considered, $\lambda_1=-2C_f\beta$ and $g_{10}=\beta C_f(F^2+A+1)$, where A is the lateral slope factor. The dotted line in Fig. 1 refers to Eq. (12). Its behavior follows the one obtained for the fourth-order model for $\delta<0$ quite well, but it gives an underestimation for high aspect ratios ($\delta>0$). This can be ascribed to the incapacity of all first-order models to recognize the resonance mechanisms between curvature and bed topography, so they work badly in superresonant conditions. On the contrary, the second-order JP model provides very similar behavior of ω_{0i} to the ZS one, as the curve is practically coincident with the bold line in Fig. 1.

A further description of the convective nature of meandering instability is given by the behavior of the temporal growth rate $\sigma(V)$ along each ray $s/\tau=V$ for different values of δ, as reported in Fig. 2. In agreement with the previous

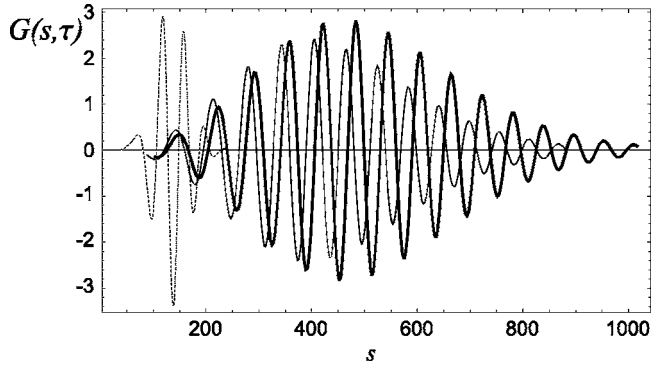

FIG. 4. Comparison of Green's function provided by different models ($\tau^*=0.1$, $\delta=-0.25$, $d_s=0.01$, $\tau=180$). The ZS model, bold line; the JP model, thin line; the IPS model, dotted line. Abscissa and ordinates appear in different scales.

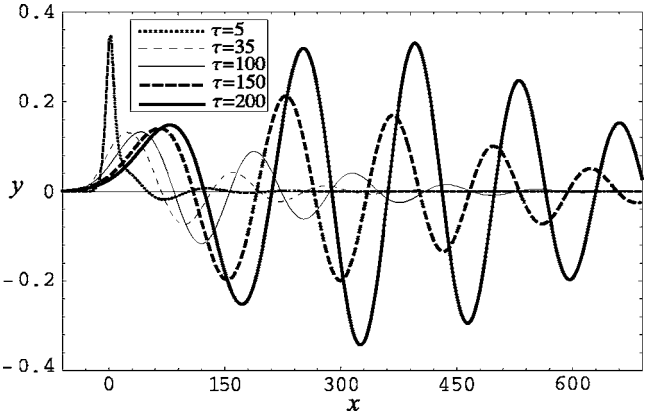

FIG. 5. Numerical simulation of the planimetric evolution consequent to an initial sharp localized perturbation in $x=0$, provided by the ZS model and using $m=0,1,2$ ($d_s=0.01$, $\delta=-0.4$, $\tau^*=0.12$). Abscissa and ordinate are made dimensionless by b and the magnitude of the initial perturbation, respectively.

considerations, it can be observed that a positive growth rate is developed alternatively either for positive or for negative values of V, depending on the aspect ratio. Therefore, a simultaneous upstream and downstream propagation is precluded. It follows that an impulsive perturbation cannot spread to the entire spatial domain but it is instead taken away; therefore, the instability is convective. Hence, as suggested by the peak location of the curves in Fig. 2, under subresonant (superresonant) conditions, the instability migrates downstream (upstream). This could be related to the results of previous experimental and theoretical investigations concerning the upstream (downstream) skewness of meanders [16,35]. Moreover, the superresonant conditions lead to greater growth rates and a wider range of unstable rays s/τ. Finally, in both cases, the range and the amplitude of instability grow as the resonance condition is approached (i.e., $|\delta| \to 0$).

IV. GREEN'S FUNCTION

In this section the long-term behavior of the solution of Eq. (9) for an initial impulsive perturbation is discussed. The generalized solution of the asymptotic approximation of Green's function obtained by Huerre [14], through the use of the method of the steepest descendent, is adopted for this purpose. In the present case, the result slightly simplifies with respect to aforementioned formula, since Eq. (9) just performs a first derivative in time and consequently the dispersion relationship is linear in ω. Thus, the asymptotic behavior of Green's function, $G(s,\tau)$, is given by

$$G(s,\tau) \simeq \frac{e^{i(k_0 s-\omega_0\tau+\pi/4)}}{i\sqrt{2\pi\tau\left(\frac{d^2\omega}{dk^2}\right)_{k_0}}}. \tag{13}$$

As far as the fourth-order ZS model is concerned, an explicit analytical expression of Eq. (13) is precluded by the high-order algebraic equation Eq. (11), which has to be solved to obtain the terms k_0. For this reason Eq. (13) has been numerically solved. On the contrary, the first- and the second-order models lead to an analytical formulation; for instance, the expression of Green's function relating to the first-order model is reported in Appendix B.

Green's function, corresponding to the fourth-order model, is shown at different times in Fig. 3 both in subresonant and superresonant conditions. The pronounced streamwise asymmetry of the wave packets can be noticed. Moreover, both the selected wavelength and the shape of the wave packet appear similar, regardless of the sign of δ, even if it depends on $|\delta|$. On the contrary, the superresonant case provides higher growth and migration rates, confirming the results of the previous section.

In order to compare the responses of linear models with different orders of complexity, Green's functions corresponding to the IPS model, the JP model and the ZS model have been displayed in Fig. 4, at time $\tau=180$. As far as the former model is concerned, we have set $A=9.75$ to obtain the same amplitude response as the ZS model. Two important considerations emerge. Firstly, the second-order model leads to a similar pattern as the fourth one even though it is slightly delayed. On the other hand, the first-order model shows a remarkable delay in the migration of the wave packet. However, it should be noticed that the time is normalized by bE/U, where the erodibility coefficient E could be fitted case-by-case in field applications. It follows that the applicative significance of the models is principally related to the shape of the wave packet response rather than to the different temporal growth rates. Secondly, the wavelengths selected by all the mathematical models agree quite well. This means that—although the time scales are different—the long-term behavior of the river planimetry could be characterized by the same dominant wavelength, without considering the higher harmonics that may be introduced by the second- and fourth-order models [36]. However, for long times, this linear description of the instability saturates due to dynamical and geometric nonlinearities that have not been considered in the present study.

Figure 5 shows the numerical simulation of the planimetric response to a sharp local perturbation. The fourth-order ZS model [i.e., Eq. (6)] has been adopted taking into account

the first three lateral modes (i.e., $m=0,1,2$). Notice that only the dynamic nonlinearities of basic Eqs. (2)–(5) are neglected in this simulation, while the geometric nonlinearities of Eq. (1) are retained by a step-to-step shifting and fitting. The numerical details are reported in Ref. [36] where, in addition, cutoff processes are also considered, and statistical comparisons with real planforms support the use of the above models to simulate long-term dynamics of meandering rivers (see also Refs. [21] and [22]).

Figure 5 underlines the convective character of the instability and suggests that it is not modified by the action of the geometric nonlinearities. Moreover, it is evident the strict similarity with the theoretical Green's function reported in Fig. 3 and it is confirmed that the second and third lateral modes do not introduce qualitative differences with respect to the behavior of the first mode.

V. CONCLUSIONS

The convective character of the linear instability that exists in the dynamics of meandering rivers has been elucidated. The convective nature emerges for all the linear morphodynamic models that were analyzed, at least in the investigated range of parameters. Therefore, the upstream propagating influence recognized by the fourth-order ZS model is not able to trigger an absolute character in the instability. The convective nature also explains the occurrence of a straight reach immediately downstream to the starting point of the river, which was detected in previous long-term numerical simulations that adopted the IPS and JP models [21,23]. The development of Green's function has shown (i) the typical shape of the wave packet that originates from the impulsive disturbance and (ii) the importance of modelling the complex fluid dynamic mechanisms involved in the meandering dynamics correctly. Finally, the above results have been confirmed by the development of a numerical simulation of the river planimetry evolution.

ACKNOWLEDGMENT

The authors would like to thank the Cassa di Risparmio di Cuneo (CRC) Foundation for financial support.

APPENDIX A: DEDUCTION OF EQ. (6)

In the following, the key steps to obtain the solution by Zolezzi and Seminara [16] are given. Firstly, the following boundary and integral conditions are imposed to Eqs. (2)–(5)

$$V = q_n = 0 \quad (n = \pm 1), \tag{A1}$$

$$\int_{-1}^{1} UDdn = 2, \quad \int_{0}^{\lambda_m}\int_{-1}^{1} (H-D)dnds = \text{const} \tag{A2}$$

where Eqs. (A1) imposes the zero-net-flux condition between the center and the sidewall layers and no sediment transport across the sidewalls, whereas Eqs. (A2) set the condition that the water discharge and the average reach slope are not influenced by perturbations in flow and topography (λ_m is a typical dimensionless wavelength).

Secondly some closure relationships for the terms τ, $\mathbf{q}$, and v_0 are required,

$$\tau_s = C_f|\mathbf{U}|U, \quad \tau_n = C_f|\mathbf{U}|\left(V + \frac{v_0(\xi_0)}{\mathcal{F}(\xi_0)}\right), \tag{A3}$$

$$q_s = q\left(\frac{\tau_s}{\tau} + K_1\frac{\tau_s\tau_n}{\beta\tau}\frac{\partial\eta}{\partial n}\right), \tag{A4}$$

$$q_n = q\left[\frac{\tau_n}{t^*} - \frac{1}{\beta}\left(K_2\frac{\tau_n^2}{\tau^2} + K_3\frac{\tau_s}{\tau}\right)\frac{\partial\eta}{\partial n}\right], \tag{A5}$$

$$v_0(\xi) = \frac{DUC}{\beta\sqrt{C_f}}G_0(\xi) + \frac{D^2(UC)_{,s}}{\beta^2 C_f}G_1(\xi) + \frac{DUCD_{,s}}{\beta^2 C_f}G_2(\xi). \tag{A6}$$

Equations (A3) assume that the dimensionless bed stress vector is aligned with the near bed velocity vector and can be expressed through a local friction coefficient. Equations (A4) and (A5) read the dynamic equilibrium of the bed sediment written in an orthogonal reference system (s,n). Finally, $\tau = |\boldsymbol{\tau}|$, $q = |\mathbf{q}|$, and K_1, K_2, and K_3 are coefficients depending on the sediment characteristics whereas the functions $G_i(\xi)$ depend on the vertical profiles $\Gamma(\xi)$ and $\mathcal{F}(\xi)$ by means of the solutions of three second order ODE's (see Ref. [16] for details).

The linearization of the morphodynamic problem can be achieved through the perturbative expansion of the previous equations, which introduced in the shallow-water Eqs. (2)–(5), leads to a linear system with four first-order differential equations.

Zolezzi and Seminara solved the linear system using a Fourier expansion in the transversal direction, n, and obtained a fourth-order ordinary differential equation (ODE) for every Fourier mode. In particular, the equation for the streamwise velocity, $u = \Sigma_{m=0}^{\infty} u_m \sin(Mn)$, gives

$$\sum_{j=0}^{4}\sigma_j\frac{d^{(j)}u_m}{ds^{(j)}} = A_m\sum_{j=0}^{4}\rho_{j+1}\frac{d^{(i)}C}{ds^{(j)}}, \tag{A7}$$

which is satisfied by the solution (6). The algebraic relationships between the coefficients σ_j, ρ_j, g_{jp}, and the river characteristics are given in Ref. [16].

APPENDIX B: GREEN'S FUNCTION FOR FIRST-ORDER MODELS

$$G(s,\tau) \simeq \frac{a\epsilon_0\sqrt{3\alpha_2^3}}{2}\frac{\exp\left[\frac{1}{6}(\alpha_0+\epsilon_2+\delta)\left\{s-\tau\left(\frac{\alpha_1-\delta}{6}-\frac{6a\epsilon_0^2}{\epsilon_0-\alpha_0+\delta}\right)+\frac{3}{2}\pi i\right\}\right]}{\sqrt{(9a^2\epsilon_0^2\alpha_2^3-\alpha_3^2\beta_0\tau^2)i\pi\tau}}, \tag{B1}$$

where

$$\alpha_0 = -3a, \quad \alpha_1 = \alpha_0 - \epsilon_0 + 6\epsilon_2^2, \quad \alpha_2 = (\epsilon_2 - \alpha_0)\tau, \tag{B2}$$

$$\alpha_3 = \beta_1 - 3\alpha_0\epsilon_0, \quad \delta = \frac{\epsilon_0 - \alpha_0}{\beta_0} + \beta_0, \tag{B3}$$

$$\beta_0 = \epsilon_2^3 - 27a^2\epsilon_1 - 27a^3 + 3a\left(3b^2 - \frac{6bs}{\tau} + \frac{3s^2}{\tau^2} + 2\epsilon_2\beta_1\right), \tag{B4}$$

$$\beta_1 = \sqrt{3\left(\frac{27a^2s}{\tau} - 9a\epsilon_0^2 - \epsilon_0^3\right)}, \quad \epsilon_0 = \sqrt{a+b}, \tag{B5}$$

$$\epsilon_1 = b + \frac{s}{\tau}, \quad \epsilon_2 = b - \frac{s}{\tau}. \tag{B6}$$

[1] S. Ikeda and G. Parker, *River Meandering* (AGU, Water Res. Monogr., Washington, DC, 1989).
[2] G. Seminara, Meccanica **33**, 59 (1998).
[3] J. P. T. Kalkwijk and H. J. De Vriend, J. Hydraul. Res. **18**, 327 (1980).
[4] G. Seminara and L. Solari, Water Resour. Res. **34**, 1585 (1998).
[5] W. E. Dietrich and J. D. Smith, Water Resour. Res. **19**, 1173 (1983).
[6] A. D. Howard, in *River Meandering*, edited by C. M. Elliott (ASCE, New York, 1984), pp. 952–963.
[7] G. Parker, K. Sawai, and S. Ikeda, J. Fluid Mech. **115**, 303 (1982).
[8] P. Blondeaux and G. Seminara, J. Fluid Mech. **157**, 449 (1985).
[9] S. G. Ikeda, G. Parker, and K. Sawai, J. Fluid Mech. **112**, 363 (1981).
[10] B. F. Edwards and D. H. Smith, Phys. Rev. E **65**, 046303 (2002).
[11] G. Parker and H. Johannesson, in *River Meandering, Water Resour. Monogr. 12*, edited by S. Ikeda and G. Parker (AGU, Washington, DC, 1989), pp. 379–415.
[12] G. Seminara, M. Tubino, and D. Zardi, in *XXIV Convegno Di Idraulica e Costruzioni Idrauliche, Napoli, 20–22 Settembre* (1994) (in Italian).
[13] A. Bers, in *Handbook of Plasma Physics*, edited by M. Rosenbluth and R. Sagdeev (North-Holland, Amsterdam 1983), pp. 451–517.
[14] P. Huerre, in *Instabilities and Nonequilibrium Structures*, edited by E. Tirapeguei and D. Villaroel (Dordrecht, Reidel, 1987), pp. 141–177.
[15] P. Huerre, in *Perspectives in Fluid Dynamics: A Collective Introduction to Current Research*, edited by J. K. Batchelor, H. Moffat, and M. G. Worster (CUP, Cambridge, 2000), pp. 159–229.
[16] G. Zolezzi and G. Seminara, J. Fluid Mech. **438**, 183 (2001).
[17] P. M. Morse and H. Feshbach, *Methods of Theoretical Physics* (McGraw-Hill, 1953).
[18] B. Federici and G. Seminara, J. Fluid Mech. **487**, 125 (2004).
[19] H. Johannesson and G. Parker, in *River Meandering, Water Resour. Monogr. 12*, edited by S. Ikeda and G. Parker (AGU, Washington, DC, 1989), pp. 181–214.
[20] A. D. Howard, in *Lowland Floodplain Rivers: Geomorphological Perspectives*, edited by P. A. Carling and G. E. Petts (John Wiley and Sons Ltd, New York, 1992), pp. 1–41.
[21] H. H. Stølum, Science **271**, 1710 (1996).
[22] T. Sun, T. Jøssang, P. Meakin, and K. Schwarz, Water Resour. Res. **32**, 2937 (1996).
[23] T. Sun, P. Meakin, and T. Jøssang, Water Resour. Res. **37**, 2227 (2001).
[24] R. C. Brower, D. A. Kessler, J. Koplik, and H. Levine, Phys. Rev. A **29**, 1335 (1984).
[25] K. Nakayama, H. Segur, and M. Wadati, Phys. Rev. Lett. **69**, 2603 (1992).
[26] M. De Vries, in *Proc. 11th Congress IAHR, Leningrad* (1965).
[27] J. Pizzuto and T. Meckelnburg, Water Resour. Res. **25**, 1005 (1989).
[28] G. Parker, P. Diplas, and J. Akiyama, J. Hydraul. Eng. **109**, 1323 (1983).
[29] G. Parker and E. D. Andrews, J. Fluid Mech. **162**, 139 (1986).
[30] A. J. Odgaard, J. Hydraul. Eng. **112**, 1117 (1986).

[31] F. M. Exner, *Uber Die Wechselwirkung Zwischen Wasser und Geschiebe in Flussen* (Sitzer Akad. Wiss, Vienna, 1925), pp. 165–180.

[32] M. Do Carmo, *Differential Geometry of Curves and Surface* (Prentice-Hall, New Jersey, 1976).

[33] P. Huerre and P. A. Monkevitz, Annu. Rev. Fluid Mech. **22**, 473 (1990).

[34] R. J. Briggs, *Electron-Stream Interaction with Plasma* (M.I.T Press, Boston, 1964).

[35] M. Colombini, M. Tubino, and P. Whiting, in *Dynamics of Gravel-Bed Rivers*, edited by P. Billi, D. D. Hey, C. R. Thorne, and P. Tacconi (John Wiley, New York, 1992), pp. 457–479.

[36] C. Camporeale, P. Perona, A. Porporato, and L. Ridolfi, Water Resour. Res. **41**, W12403 (2005).